

## Giant Anisotropy of Spin Relaxation and Spin-Valley Mixing in a Silicon Quantum Dot

Xin Zhang,<sup>1,2,\*</sup> Rui-Zi Hu<sup>1,2,\*</sup>, Hai-Ou Li,<sup>1,2,†</sup> Fang-Ming Jing,<sup>1,2</sup> Yuan Zhou,<sup>1,2</sup> Rong-Long Ma<sup>1,2</sup>, Ming Ni,<sup>1,2</sup> Gang Luo,<sup>1,2</sup> Gang Cao,<sup>1,2</sup> Gui-Lei Wang,<sup>3</sup> Xuedong Hu,<sup>4</sup> Hong-Wen Jiang,<sup>5</sup> Guang-Can Guo,<sup>1,2</sup> and Guo-Ping Guo<sup>1,2,6,‡</sup>

<sup>1</sup>CAS Key Laboratory of Quantum Information, University of Science and Technology of China, Hefei, Anhui 230026, China

<sup>2</sup>CAS Center for Excellence and Synergetic Innovation Center in Quantum Information and Quantum Physics, University of Science and Technology of China, Hefei, Anhui 230026, China

<sup>3</sup>Key Laboratory of Microelectronics Devices & Integrated Technology, Institute of Microelectronics, Chinese Academy of Sciences, Beijing 100029, China

<sup>4</sup>Department of Physics, University at Buffalo, SUNY, Buffalo, New York 14260, USA

<sup>5</sup>Department of Physics and Astronomy, University of California, Los Angeles, California 90095, USA

<sup>6</sup>Origin Quantum Computing Company Limited, Hefei, Anhui 230026, China

 (Received 11 December 2019; revised manuscript received 20 April 2020; accepted 19 May 2020; published 23 June 2020)

In silicon quantum dots (QDs), at a certain magnetic field commonly referred to as the “hot spot,” the electron spin relaxation rate ( $T_1^{-1}$ ) can be drastically enhanced due to strong spin-valley mixing. Here, we experimentally find that with a valley splitting of  $78.2 \pm 1.6 \mu\text{eV}$ , this hot spot in spin relaxation can be suppressed by more than 2 orders of magnitude when the in-plane magnetic field is oriented at an optimal angle, about  $9^\circ$  from the [100] sample plane. This directional anisotropy exhibits a sinusoidal modulation with a  $180^\circ$  periodicity. We explain the magnitude and phase of this modulation using a model that accounts for both spin-valley mixing and intravalley spin-orbit mixing. The generality of this phenomenon is also confirmed by tuning the electric field and the valley splitting up to  $268.5 \pm 0.7 \mu\text{eV}$ .

DOI: 10.1103/PhysRevLett.124.257701

Single-spin qubits in Si quantum dots (QDs) are considered one of the most promising contenders for large scale quantum computation [1–3]. In silicon, the relatively weak spin-orbit interaction (SOI) and the existence of an abundant spin-zero isotope allow the electron spin to preserve its quantum state for exceptionally long times, leading to a spin relaxation time ( $T_1$ ) over hundreds of milliseconds [4–6] and a spin coherence time ( $T_2$ ) over tens of microseconds [7,8]. However, adverse effects from an imperfect substrate may weaken some of these advantages [2]. In silicon QDs, the energy gap between the lowest two valley-orbit states, which are obtained by breaking sixfold degeneracy of the conduction band minima (valley), is sensitive to the interface disorder [9–12]. For spin relaxation, this energy gap, also called valley splitting, introduces a spin relaxation “hot spot” when its magnitude  $E_{\text{VS}}$  matches the Zeeman energy  $E_Z$  [13]. As a result, the spin relaxation rate can be enhanced to  $10^3$  to  $10^6 \text{ s}^{-1}$  [6,14–16] depending on the environment. To mitigate such effects, it is crucial to better understand and control the interactions between the spin and valley degrees of freedom in silicon.

Over the past decade, spin relaxation in Si QDs has been investigated both experimentally [4–6,14–17] and theoretically [13,18,19]. It was found that electrical noise via SOI plays an important role in determining spin relaxation in silicon. For magnetic fields near the spin relaxation hot spot, the relaxation process is dominated by the SOI with valley states (spin-valley mixing), while for magnetic fields

away from the hot spot, especially higher fields,  $T_1$  is dominated by the intravalley SOI with higher orbital states (intravalley spin-orbit mixing). The effect of SOI on spin relaxation can be viewed as a result of an effective spin-orbit magnetic field  $\mathbf{B}_{\text{SO}}$ . A finite angle between  $\mathbf{B}_{\text{SO}}$  and the external magnetic field  $\mathbf{B}_{\text{ext}}$  leads to mixing of spin eigenstates [20,21], allowing electrical noises to induce spin transitions between the excited and ground states. Within this physical picture, spin mixing would vary as the angle between  $\mathbf{B}_{\text{SO}}$  and  $\mathbf{B}_{\text{ext}}$  is changed. Therefore,  $T_1^{-1}$  should be anisotropic with respect to the external magnetic field direction.

Previous studies have revealed an anisotropic  $T_1^{-1}$  in GaAs QDs [22,23] and a tunable SOI in silicon using the magnetic field direction [24,25], but so far, an anisotropic  $T_1^{-1}$  in Si QDs has not been investigated. Indeed,  $T_1^{-1}$  anisotropy could help improve the relaxation performance of a certain qubit by choosing an optimized magnetic field orientation. Furthermore, it is also a probe into the anisotropy of both spin-valley mixing and intravalley spin-orbit mixing.

Here, we investigate extensively the spin relaxation anisotropy near the hot spot in a Si metal-oxide-semiconductor (MOS) QD. We find that with  $E_{\text{VS}} = 78.2 \pm 1.6 \mu\text{eV}$ , the variation in  $T_1^{-1}$  can be as large as 2 orders of magnitude at 0.8 T, but is significantly suppressed at 1.5 T. Based on a model of multiple relaxation channels and a modified picture of the effective spin-orbit magnetic field,

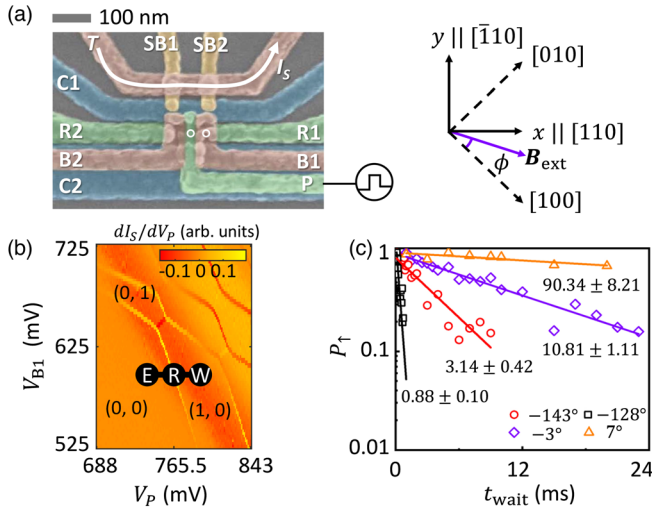


FIG. 1. (a) Scanning electron microscope image of a DQD device identical to the one measured. Two circles are used to proportionally denote the position and size of the dots. Inset: the crystallographic directions with respect to the sample. (b) Charge stability diagram of the DQD. The relative voltage magnitude at each step of the pulse sequence for measuring  $T_1$  is overlaid on the data. (c) Normalized spin-up fraction as a function of the waiting time  $t_{\text{wait}}$  for different angles  $\phi$  of the 0.8 T in-plane magnetic field with  $E_{\text{VS}} = 78.2 \pm 1.6 \mu\text{eV}$ . The solid lines are exponential fits to the data with the values of  $T_1$  (ms) indicated aside.

we explain our observations by identifying the limiting mechanisms of spin-valley mixing and intravalley spin-orbit mixing. We also tune the gate voltage to examine the effect of interface electric field, and find that even if the valley splitting is increased to  $268.5 \pm 0.7 \mu\text{eV}$  by tuning the electric field, the variation range in  $T_1^{-1}$  can still be up to nearly 2 orders of magnitude, with the minimal relaxation angle shifted from  $8.9 \pm 0.8^\circ$  to  $1.8 \pm 2.4^\circ$ . Overall, our results should provide useful guidance for future research on spin-valley mixing and spin control experiments.

The experiment is carried out in a Si-MOS double quantum dot (DQD) device [Fig. 1(a)], though we use only one QD for  $T_1$  measurements. The device is fabricated from an 8-in natural silicon wafer grown by the float zone method, which is near intrinsic and has high resistivity ( $>10 \text{ k}\Omega/\text{cm}^2$ ) [26]. Four layers of overlapping aluminum gates with insulating oxide in between are employed to laterally confine the QDs [26,27] (see Supplemental Material [28], Sec. 1). During the experiment, gates  $T$ ,  $\text{SB1}$ , and  $\text{SB2}$  are used to define a single electron transistor (SET) to monitor the charge state of the DQD. By differentiating the SET current  $I_S$  with respect to gate voltages  $V_P$  and  $V_{B1}$ , a charge stability diagram can be obtained [Fig. 1(b)]. Here, we use (NL, NR) to refer to the number of electrons in the dot under gates  $P$  and  $B1$ , respectively, and we perform the spin relaxation measurements near the  $(0, 0)$ - $(1, 0)$  charge transition far detuned from the interdot

transition  $(0, 1)$ - $(1, 0)$ , which allows us to treat the left QD as an isolated QD. The orientation of the QD gate pattern with respect to the main crystallographic directions is also shown in Fig. 1(a) and we apply an in-plane magnetic field at an angle  $\phi$  from the  $[100]$  direction. For the convenience of discussion, we define  $[110]$  and  $[\bar{1}10]$  to be the  $x$  and  $y$  axes, respectively.

To measure spin relaxation time  $T_1$ , we apply to gate  $P$  a three-step pulse sequence that was first implemented by Elzerman *et al.* [35], as shown by points  $E$  (empty),  $R$  (read), and  $W$  (wait) in Fig. 1(b): first, at point  $W$  an electron is injected into the QD with a random spin state and after a time  $t_{\text{wait}}$ , the spin state is read out via spin-to-charge conversion by pulsing to point  $R$ , finally, the QD is emptied at point  $E$ . By measuring the spin-up probability as a function of  $t_{\text{wait}}$  and fitting the data with an exponential decay, we can extract the value of  $T_1$ . Some examples of the exponential decays of the normalized spin-up probability  $P_\uparrow$  from the experiments can be seen in Fig. 1(c), showing a striking variation in  $T_1$  upon rotating the magnetic field orientation. The experimental details of the  $T_1$  measurements and device parameter extraction are described in Supplemental Material [28], Secs. 2 and 3.

The measured  $T_1^{-1}$  as a function of the magnetic field oriented along the direction of  $\phi = 117^\circ$  is presented in Fig. 2(a), showing a typical spin relaxation hot spot with  $E_{\text{VS}} = 78.2 \pm 1.6 \mu\text{eV}$ . By rotating the in-plane magnetic field orientation over the whole  $360^\circ$  range with a constant strength of 0.8 and 1.5 T, we observe a sinusoidal modulation of the spin relaxation rate with a  $180^\circ$  periodicity. Interestingly, as shown in Fig. 2(b), while the data for the two different magnetic field strengths show a nearly common minima angle of  $8.9 \pm 0.8^\circ$  with respect to the  $[100]$  plane (see Supplemental Material, Sec. 8), the variation ranges are significantly different: for 0.8 T,  $T_1^{-1}$  varies by more than 2 orders of magnitude, which is approximately 1 order of magnitude larger than that in GaAs QDs [22,23], while for 1.5 T, the variation range decreases to only six times.

To understand these distinctive behaviors of the  $T_1^{-1}$  anisotropy, we first identify different origins of spin relaxation in silicon [13,15]. The expression for  $T_1^{-1}$  can be written as a sum of various contributions

$$T_1^{-1} = \Gamma_{J,\text{SV}} + \Gamma_{\text{ph},\text{SV}} + \Gamma_{J,\text{SO}} + \Gamma_{\text{ph},\text{SO}} + \Gamma_{\text{const}}, \quad (1)$$

where subscripts ‘‘SV’’ and ‘‘SO’’ denote spin-valley mixing and intravalley spin-orbit mixing, while subscript ‘‘J’’ or ‘‘ph’’ indicates that the type of electrical noise facilitating spin relaxation is Johnson noise or phonon noise. Different types of noise give the spin relaxation rate different power law dependences on the Zeeman energy (see Supplemental Material [28], Sec. 7) [13]. Finally,  $\Gamma_{\text{const}}$  describes a relaxation channel that is independent of (or at least insensitive to) the external magnetic field [15]. By

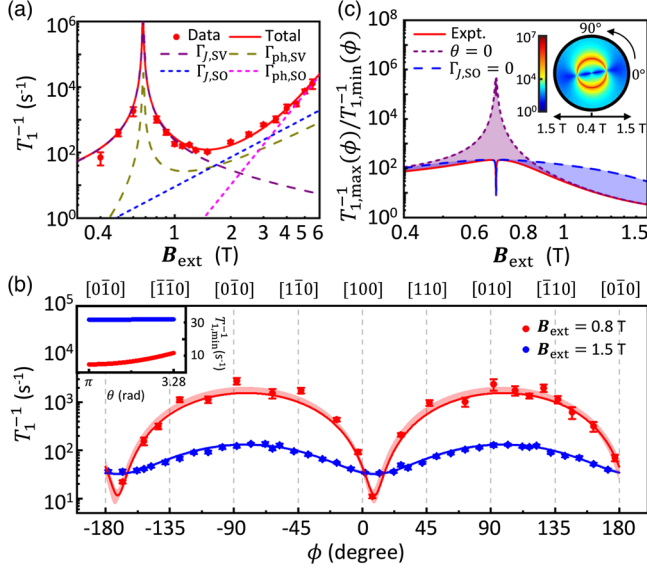


FIG. 2. (a) Relaxation rates as a function of the magnetic field strength with an in-plane angle of  $\phi = 117^\circ$ . The fittings include contributions from different relaxation channels obtained through the model discussed in the main text. (b) Angular dependence of the relaxation rate measured with different magnetic field strengths. The red and blue solid lines are numerical results based on the spin relaxation model and the parameters from experiment, while the corresponding shaded areas indicate a 95% confidence interval with a sinusoidal fit. Inset:  $T_{1,\min}^{-1}(\phi)$  as a function of the parameter  $\theta$  for  $B_{\text{ext}} = 0.8$  T (red) and  $B_{\text{ext}} = 1.5$  T (blue). (c) Anisotropy magnitude as a function of the magnetic field strength under real experimental conditions or certain assumptions. The shaded areas indicate the amount of anisotropy suppressed by corresponding mechanism. Inset: numerical simulation of the spin relaxation hot spot as a function of the external magnetic field angle.

including all the major contributions to spin relaxation, we can fit the experimental data really well, and can identify the dominant relaxation channel at different field ranges, as illustrated in Fig. 2(a). In general, spin-valley mixing and intravalley spin-orbit mixing dominate spin relaxation for  $B_{\text{ext}} < 1.5$  T and  $B_{\text{ext}} > 1.5$  T, respectively, and  $\Gamma_{\text{const}}$  is negligibly small for most external fields ( $B_{\text{ext}} > 0.4$  T). More specifically, for  $1.5 \text{ T} < B_{\text{ext}} < 3$  T,  $\Gamma_{J,\text{SO}}$  is much greater than  $\Gamma_{\text{ph},\text{SO}}$ . Therefore, the giant  $T_1^{-1}$  anisotropy at  $B_{\text{ext}} = 0.8$  T is most probably due to anisotropic spin-valley mixing, which is largely suppressed by the fast increase in  $\Gamma_{J,\text{SO}}$  at  $B_{\text{ext}} = 1.5$  T. In the latter case, the anisotropy of  $\Gamma_{J,\text{SO}}$  may play a role. However, since we do not observe an apparent angle shift of the anisotropy curve from 0.8 to 1.5 T, its effect may still be negligible.

With the anisotropy of spin-valley mixing the probable cause for spin relaxation anisotropy at 0.8 T, we now examine this mechanism in more detail. It is useful to reconsider the intuitive picture of the interplay between  $\mathbf{B}_{\text{SO}}$  and  $\mathbf{B}_{\text{ext}}$  [20,21]. As shown in Fig. 3(a), the presence of  $\mathbf{B}_{\text{SO}}$

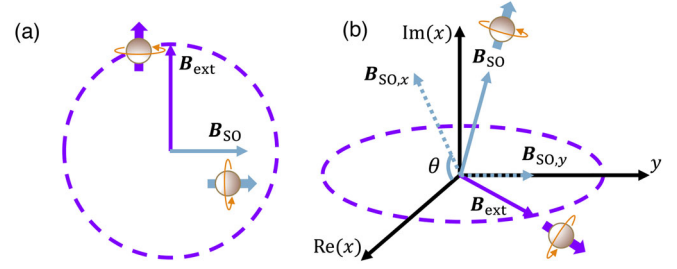


FIG. 3. (a) Illustration of the intuitive classical picture of the interaction between the effective spin-orbit magnetic field  $\mathbf{B}_{\text{SO}}$  and the external magnetic field  $\mathbf{B}_{\text{ext}}$ . The dashed circle shows the rotation of  $\mathbf{B}_{\text{ext}}$ . (b) Modified intuitive picture of the interaction between  $\mathbf{B}_{\text{SO}}$  and  $\mathbf{B}_{\text{ext}}$ .

causes the spin to precess around an axis different from that of  $\mathbf{B}_{\text{ext}}$ , creating a channel for the spin to relax. If  $\mathbf{B}_{\text{SO}}$  is a real magnetic field, this spin-mixing effect would be maximum when  $\mathbf{B}_{\text{SO}} \perp \mathbf{B}_{\text{ext}}$  and is zero when  $\mathbf{B}_{\text{SO}} \parallel \mathbf{B}_{\text{ext}}$ . As a result, the extrema position should be determined by the direction of  $\mathbf{B}_{\text{SO}}$  and there are two opportunities in the whole rotation range for  $\mathbf{B}_{\text{ext}}$  to be parallel or perpendicular to  $\mathbf{B}_{\text{SO}}$ , leading to a modulation cycle of  $180^\circ$ , which is consistent with the experimental results. However, within this simple geometric picture spin relaxation due to spin-valley mixing should be completely suppressed when the two fields are in parallel, leading to a much larger degree of anisotropy in  $T_1^{-1}$ , which is obviously not what we observed. To address this issue, we revisit the intervalley spin-orbit Hamiltonian, from which  $\mathbf{B}_{\text{SO}}$  for spin-valley mixing can be expressed as (see also Supplemental Material [28], Sec. 6) [6,13]

$$\mathbf{B}_{\text{SO}} = \frac{im^* E_{\text{VS}}}{\hbar\gamma} (\alpha_m r_y^- \hat{x} + \alpha_p r_x^+ \hat{y}). \quad (2)$$

Here,  $\gamma$  is the gyromagnetic ratio,  $\alpha_m = \beta - \alpha$  and  $\alpha_p = \beta + \alpha$  are the SOI constants from the Dresselhaus SOI ( $\beta$ ) and Rashba SOI ( $\alpha$ ), and  $r_y^-$  ( $r_x^+$ ) represents the intervalley dipole matrix element between the two valley eigenstates along the  $y$  ( $x$ ) axis. In general,  $r_y^-$  and  $r_x^+$  are complex numbers (see Supplemental Material [28], Sec. 6), so that the effective spin-orbit magnetic fields are also complex. To quantify the contribution of the complex terms, we introduce a complex number  $\mathbf{R} = \mathbf{B}_{\text{SO},x} / \mathbf{B}_{\text{SO},y} = \alpha_m r_y^- / \alpha_p r_x^+ = R e^{i\theta}$ , where  $R$  is the absolute value and  $\theta$  is the phase. Assuming that  $\mathbf{B}_{\text{SO},y}$  is fully real and  $\mathbf{B}_{\text{SO},x}$  is complex with a phase  $\theta$ , the total spin-orbit field  $\mathbf{B}_{\text{SO}}$  can then be represented by a vector in three-dimensional space with an extra axis referring to the imaginary part of  $\mathbf{B}_{\text{SO},x}$  [see Fig. 3(b)], with angle  $\theta$  between  $\mathbf{B}_{\text{SO},x}$  and the  $x$  axis. A finite  $\theta$  shifts  $\mathbf{B}_{\text{SO},x}$  away from the  $x$ - $y$  plane, so that  $\mathbf{B}_{\text{ext}}$  in the two-dimensional plane would never be parallel to  $\mathbf{B}_{\text{SO}}$ , resulting in a residual SOI induced  $T_1^{-1}$  when  $\mathbf{B}_{\text{ext}}$  is along

the minimum angle. Conversely, if the angle  $\theta$  can be tuned, it would enable control of the magnitude of the spin mixing and relaxation anisotropy. Based on the parameters extracted from Fig. 2(a), a numerical calculation of  $T_1^{-1}$  (see Supplemental Material [28], Sec. 7) produces a best fit with the data in Fig. 2(b) when  $\theta = 3.28$  rad and  $R = 1.35$ . The nonzero imaginary part brought by  $\theta$  leads to a reduced anisotropy of spin-valley mixing and causes a nonvanishing hot spot when rotating the magnetic field orientation. This can be seen by the calculated hot spot over the whole  $360^\circ$  range in the inset of Fig. 2(c). Notice other relaxation channels such as  $\Gamma_{J,SO}$ ,  $\Gamma_{ph,SO}$ , and  $\Gamma_{const}$  cannot cause such a nonvanishing hot spot because the hot spot is only determined by spin-valley mixing. In Supplemental Material [28], Sec. 7, we show that the angle of the minimal relaxation rate is also determined by the complex number  $\mathbf{R}$ . It should be noted that the  $8.9^\circ \pm 0.8^\circ$  angular deviation from [100] direction may also arise from systematic errors such as an inaccuracy in measuring the sample orientation. However, we estimate these errors together to be no more than  $\pm 3^\circ$  (see Supplemental Material [28], Sec. 2). Therefore, this deviation angle is a clear reflection of the complex nature of spin-valley mixing.

To identify the limiting mechanisms at different magnetic fields for the spin relaxation anisotropy, we numerically calculate the anisotropy magnitude  $T_{1,max}^{-1}(\phi)/T_{1,min}^{-1}(\phi)$ . As shown in Fig. 2(c), the variation range is mostly limited by  $\theta$  from spin-valley mixing for  $\mathbf{B}_{ext} < 0.85$  T, and by the residual relaxation rate  $\Gamma_{J,SO}$  for  $\mathbf{B}_{ext} > 0.85$  T. These conclusions are also illustrated in the inset of Fig. 2(b), if  $\theta$  was set to  $\pi$ , that is,  $\mathbf{R}$  is a real number,  $T_{1,min}^{-1}(\phi)$  would have been further reduced for  $\mathbf{B}_{ext} = 0.8$  T, but remained nearly the same for  $\mathbf{B}_{ext} = 1.5$  T. Notice in Fig. 2(c), the limiting mechanism of  $\Gamma_{ph,SO}$  is not considered since its magnitude is much smaller than that of  $\Gamma_{J,SO}$  for the range of magnetic field.

According to previous studies [6,36], the valley splitting and the valley-dependent SOI constants are dependent on the applied electric field in Si MOS QDs. Here, we examine how the interface electric field affects  $T_1^{-1}$  anisotropy via spin-valley mixing. As shown in Fig. 4(a), the valley splitting in our device does increase almost linearly with  $V_p$  (for the measurement of the valley splitting, see Supplemental Material [28], Sec. 4). We then investigate the behavior of  $T_1^{-1}$  anisotropy with  $E_{VS}$  increased to  $268.5 \pm 0.7 \mu\text{eV}$ . The measured  $T_1^{-1}(\mathbf{B}_{ext})$  along the direction of  $\phi = 117^\circ$  and  $\phi = -178^\circ$  (near the minimum  $T_1^{-1}$  direction, see Supplemental Material [28], Sec. 5) and the calculated hot spot variation by rotating magnetic field are shown in Fig. 4(b). While the hot spot anisotropy magnitude is similar to that in Fig. 2(c), the extrema position is shifted from  $8.9 \pm 0.8^\circ$  to  $1.8 \pm 2.4^\circ$ . This can be explained by the variation of  $\mathbf{R}$  due to the electric field change. To

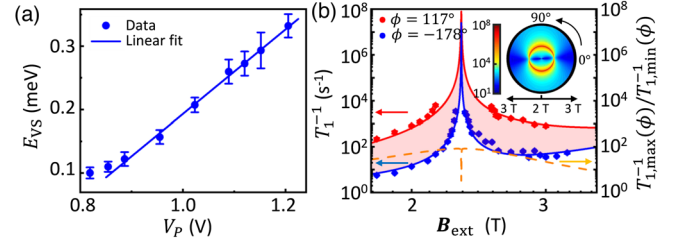


FIG. 4. (a) Valley splitting  $E_{VS}$  as a function of the gate voltage  $V_p$ . A linear fit shows a tunability of  $0.667 \pm 0.020$  meV  $V^{-1}$ . The deviation from the linear fit at small  $V_p$  perhaps results from an interface localized interaction [36]. (b) Relaxation rates as a function of the external magnetic field along different directions and the calculated anisotropy magnitude with experimental parameters. Solid lines are numerical results based on our spin relaxation model and the parameters from experiment. Inset: numerical simulation of the spin relaxation hot spot as a function of the orientation of the external magnetic field.

achieve best fit with the data,  $\theta$  and  $R$  in our model have to be changed to 3.36 rad and 1.1, respectively. According to previous studies, the origin of this change can be the electric field effect on the QD shape [37], SOI constants [38], or the relative position between the QD and an interfacial step [24,39]. Further insights into the electrical field effect can be obtained by independently verifying the variation of valley-dependent SOI and intervalley transition elements. Overall, the increased electric field leads to moderate changes in both the magnitude and the orientation of  $T_1^{-1}$  anisotropy, but the basic features of the giant  $T_1^{-1}$  anisotropy remain even though the valley splitting is increased by over 2 times.

In the discussion above, the complex SOI field plays a significant role in determining the  $T_1^{-1}$  anisotropy caused by spin-valley mixing, although the exact value of the SOI strength  $\alpha_m/\alpha_p$  and the intervalley transition matrix elements  $r_y^+/r_x^+$  cannot be distinguished. To extract their values, more information is needed, such as the physical mechanism of the intervalley transition elements and their dependence on the electric and magnetic fields [10,12,36,40,41]. Nevertheless, the modified picture of a complex  $\mathbf{B}_{SO}$  mixing the spin eigenstates of  $\mathbf{B}_{ext}$  helps us determine both the magnitude and orientation of the anisotropic spin-valley mixing, which is a clear indication that  $T_1^{-1}$  anisotropy is an effective approach for characterizing spin-valley mixing in silicon. Moreover, the large anisotropy of the spin relaxation hot spot observed in this work also provides a method to suppress  $T_1^{-1}$  in silicon QDs, which would in turn allow a larger magnetic field range for high fidelity readout and control of qubits. Such an increased workable field range may specifically inspire experiments in Si/SiGe heterostructure QDs where the valley splitting may be less controllable [15,16]. Additionally, the great modulation of spin-valley mixing may create new ways to optimize qubit performance,

especially for qubits driven by spin-orbit coupling [39,42,43] (see Supplemental Material [28], Sec. 9).

In conclusion, we have studied how spin relaxation in silicon depends sensitively on the external field orientation. By rotating an in-plane magnetic field, we find that the spin relaxation rate near the spin-valley hot spot can be reduced by more than 2 orders of magnitude. The range of this large variation is found to be controlled both by spin-valley mixing and intravalley spin-orbit mixing. We have also shown that this great anisotropy holds in a larger electric field with slightly varied parameters of spin-valley mixing compared to the significant increase of valley splitting. For future work, the anisotropy of intravalley spin-orbit mixing at much larger magnetic fields could be investigated, which should offer a deeper understanding of the mechanism for SOI with valley and orbital states in silicon.

We acknowledge P. Huang for helpful discussions of spin-valley relaxation. And we acknowledge D. Culcer and Z. Wang for helpful discussions of the mechanism of spin-orbit coupling. Research was supported by the National Key Research and Development Program of China (Grant No. 2016YFA0301700), the National Natural Science Foundation of China (Grants No. 61674132, No. 11674300, and No. 11625419), the Strategic Priority Research Program of the CAS (Grant No. XDB24030601), the Anhui initiative in Quantum Information Technologies (Grant No. AHY080000), and this work was partially carried out at the USTC Center for Micro and Nanoscale Research and Fabrication. G.-L. W. acknowledges financial support by the Youth Innovation Promotion Association of the Chinese Academy of Sciences under Grant No. 2016112. H.-W.J. and X.H. acknowledge financial support by U.S. ARO through Grant No. W911NF1410346 and No. W911NF1710257, respectively.

\*These authors contributed equally to this work.

<sup>†</sup>haiouli@ustc.edu.cn

<sup>‡</sup>gpguo@ustc.edu.cn

- [1] R. Hanson, L. P. Kouwenhoven, J. R. Petta, S. Tarucha, and L. M. K. Vandersypen, *Rev. Mod. Phys.* **79**, 1217 (2007).
- [2] F. A. Zwanenburg, A. S. Dzurak, A. Morello, M. Y. Simmons, L. C. L. Hollenberg, G. Klimeck, S. Rogge, S. N. Coppersmith, and M. A. Eriksson, *Rev. Mod. Phys.* **85**, 961 (2013).
- [3] X. Zhang, H.-O. Li, G. Cao, M. Xiao, G.-C. Guo, and G.-P. Guo, *Natl. Sci. Rev.* **6**, 32 (2018).
- [4] M. Xiao, M. G. House, and H. W. Jiang, *Phys. Rev. Lett.* **104**, 096801 (2010).
- [5] C. B. Simmons, J. R. Prance, B. J. Van Bael, T. S. Koh, Z. Shi, D. E. Savage, M. G. Lagally, R. Joynt, M. Friesen, S. N. Coppersmith, and M. A. Eriksson, *Phys. Rev. Lett.* **106**, 156804 (2011).
- [6] C. Yang, A. Rossi, R. Ruskov, N. Lai, F. Mohiyaddin, S. Lee, C. Tahan, G. Klimeck, A. Morello, and A. Dzurak, *Nat. Commun.* **4**, 2069 (2013).
- [7] M. Veldhorst, J. C. C. Hwang, C. H. Yang, A. W. Leenstra, B. de Ronde, J. P. Dehollain, J. T. Muhonen, F. E. Hudson, K. M. Itoh, A. Morello, and A. S. Dzurak, *Nat. Nanotechnol.* **9**, 981 (2014).
- [8] E. Kawakami, P. Scarlino, D. R. Ward, F. R. Braakman, D. E. Savage, M. G. Lagally, M. Friesen, S. N. Coppersmith, M. A. Eriksson, and L. M. K. Vandersypen, *Nat. Nanotechnol.* **9**, 666 (2014).
- [9] L. J. Sham and M. Nakayama, *Phys. Rev. B* **20**, 734 (1979).
- [10] A. L. Saraiva, M. J. Calderón, X. Hu, S. Das Sarma, and B. Koiller, *Phys. Rev. B* **80**, 081305(R) (2009).
- [11] M. Friesen and S. N. Coppersmith, *Phys. Rev. B* **81**, 115324 (2010).
- [12] D. Culcer, X. Hu, and S. Das Sarma, *Phys. Rev. B* **82**, 205315 (2010).
- [13] P. Huang and X. Hu, *Phys. Rev. B* **90**, 235315 (2014).
- [14] L. Petit, J. M. Boter, H. G. J. Eenink, G. Droulers, M. L. V. Tagliaferri, R. Li, D. P. Franke, K. J. Singh, J. S. Clarke, R. N. Schouten, V. V. Dobrovitski, L. M. K. Vandersypen, and M. Veldhorst, *Phys. Rev. Lett.* **121**, 076801 (2018).
- [15] F. Borjans, D. M. Zajac, T. M. Hazard, and J. R. Petta, *Phys. Rev. Applied* **11**, 044063 (2019).
- [16] A. Hollmann, T. Struck, V. Langrock, A. Schmidbauer, F. Schauer, T. Leonhardt, K. Sawano, H. Riemann, N. V. Abrosimov, D. Bougeard, and L. R. Schreiber, *Phys. Rev. Applied* **13**, 034068 (2020).
- [17] R. R. Hayes, A. A. Kiselev, M. G. Borselli, S. S. Bui, E. T. Croke, III, P. W. Deelman, B. M. Maune, I. Milosavljevic, J.-S. Moon, R. S. Ross, A. E. Schmitz, M. F. Gyure, and A. T. Hunter, [arXiv:0908.0173](https://arxiv.org/abs/0908.0173).
- [18] C. Tahan and R. Joynt, *Phys. Rev. B* **89**, 075302 (2014).
- [19] P. Huang and X. Hu, *Phys. Rev. B* **89**, 195302 (2014).
- [20] P. Stano and J. Fabian, *Phys. Rev. B* **72**, 155410 (2005).
- [21] A. Hofmann, V. F. Maisi, T. Krähenmann, C. Reichl, W. Wegscheider, K. Ensslin, and T. Ihn, *Phys. Rev. Lett.* **119**, 176807 (2017).
- [22] P. Scarlino, E. Kawakami, P. Stano, M. Shafiei, C. Reichl, W. Wegscheider, and L. M. K. Vandersypen, *Phys. Rev. Lett.* **113**, 256802 (2014).
- [23] L. C. Camenzind, L. Yu, P. Stano, J. D. Zimmerman, A. C. Gossard, D. Loss, and D. M. Zumbühl, *Nat. Commun.* **9**, 3454 (2018).
- [24] R. Ferdous, E. Kawakami, P. Scarlino, M. P. Nowak, D. R. Ward, D. E. Savage, M. G. Lagally, S. N. Coppersmith, M. Friesen, M. A. Eriksson, L. M. K. Vandersypen, and R. Rahman, *npj Quantum Inf.* **4**, 26 (2018).
- [25] T. Tanttu, B. Hensen, K. W. Chan, C. H. Yang, W. W. Huang, M. Fogarty, F. Hudson, K. Itoh, D. Culcer, A. Laucht, A. Morello, and A. Dzurak, *Phys. Rev. X* **9**, 021028 (2019).
- [26] S. J. Angus, A. J. Ferguson, A. S. Dzurak, and R. G. Clark, *Nano Lett.* **7**, 2051 (2007).
- [27] K. Wang, H.-O. Li, G. Luo, X. Zhang, F.-M. Jing, R.-Z. Hu, Y. Zhou, H. Liu, G.-L. Wang, G. Cao, H.-W. Jiang, and G.-P. Guo, *Europhys. Lett.* **130**, 27001 (2020).
- [28] See Supplemental Material at <http://link.aps.org/supplemental/10.1103/PhysRevLett.124.257701> for more details on the device fabrication, the measurement setup, data analysis, equation derivations for spin-valley mixing,

- numerical calculations, and a discussion of the implications of this Letter, which includes Refs. [29–34].
- [29] A. Morello, J. J. Pla, F. A. Zwanenburg, K. W. Chan, K. Y. Tan, H. Huebl, M. Möttönen, C. D. Nugroho, C. Yang, J. A. van Donkelaar, A. D. C. Alves, D. N. Jamieson, C. C. Escott, L. C. L. Hollenberg, R. G. Clark, and A. S. Dzurak, *Nature (London)* **467**, 687 (2010).
- [30] W. H. Lim, C. H. Yang, F. A. Zwanenburg, and A. S. Dzurak, *Nanotechnology* **22**, 335704 (2011).
- [31] D. M. Zajac, T. M. Hazard, X. Mi, E. Nielsen, and J. R. Petta, *Phys. Rev. Applied* **6**, 054013 (2016).
- [32] M. Friesen, S. Chutia, C. Tahan, and S. N. Coppersmith, *Phys. Rev. B* **75**, 115318 (2007).
- [33] X. Hao, R. Ruskov, M. Xiao, C. Tahan, and H. Jiang, *Nat. Commun.* **5**, 3860 (2014).
- [34] V. N. Golovach, A. Khaetskii, and D. Loss, *Phys. Rev. Lett.* **93**, 016601 (2004).
- [35] J. M. Elzerman, R. Hanson, L. H. Willems van Beveren, B. Witkamp, L. M. K. Vandersypen, and L. P. Kouwenhoven, *Nature (London)* **430**, 431 (2004).
- [36] R. Ruskov, M. Veldhorst, A. S. Dzurak, and C. Tahan, *Phys. Rev. B* **98**, 245424 (2018).
- [37] S. Amasha, K. MacLean, I. P. Radu, D. M. Zumbühl, M. A. Kastner, M. P. Hanson, and A. C. Gossard, *Phys. Rev. Lett.* **100**, 046803 (2008).
- [38] Y. Kanai, R. S. Deacon, S. Takahashi, A. Oiwa, K. Yoshida, K. Shibata, K. Hirakawa, Y. Tokura, and S. Tarucha, *Nat. Nanotechnol.* **6**, 511 (2011).
- [39] W. Huang, M. Veldhorst, N. M. Zimmerman, A. S. Dzurak, and D. Culcer, *Phys. Rev. B* **95**, 075403 (2017).
- [40] J. K. Gamble, M. A. Eriksson, S. N. Coppersmith, and M. Friesen, *Phys. Rev. B* **88**, 035310 (2013).
- [41] B. Tariq and X. Hu, *Phys. Rev. B* **100**, 125309 (2019).
- [42] A. Corna, L. Bourdet, R. Maurand, A. Crippa, D. Kotekar-Patil, H. Bohuslavskyi, R. Laviéville, L. Hutin, S. Barraud, X. Jehl, M. Vinet, S. De Franceschi, Y.-M. Niquet, and M. Sanquer, *npj Quantum Inf.* **4**, 6 (2018).
- [43] P. Harvey-Collard, N. T. Jacobson, C. Bureau-Oxton, R. M. Jock, V. Srinivasa, A. M. Mounce, D. R. Ward, J. M. Anderson, R. P. Manginell, J. R. Wendt, T. Pluym, M. P. Lilly, D. R. Luhman, M. Pioro-Ladrière, and M. S. Carroll, *Phys. Rev. Lett.* **122**, 217702 (2019).